12-11-2002

A Simulation Study of Space-based Observations of Gravity Waves in the Airglow using Observed ALOHA-93 Wave Parameters

Michael P. Hickey Ph.D.
Embry-Riddle Aeronautical University, hicke0b5@erau.edu

J. S. Brown
Clemson University

Scholarly Commons Citation

Hickey, M. P., and J. S. Brown, A simulation study of space-based observations of gravity waves in the airglow using observed ALOHA-93 wave parameters, J. Geophys. Res., 107(A12), 1431, doi: https://doi.org/10.1029/2001JA009225

A simulation study of space-based observations of gravity waves in the airglow using observed ALOHA-93 wave parameters

M. P. Hickey[1] and J. S. Brown

Department of Physics and Astronomy, Clemson University, Clemson, South Carolina, USA

Received 19 December 2001; revised 21 May 2002; accepted 30 September 2002; published 11 December 2002.

[1] We use gravity wave parameters derived from the ALOHA-93 campaign to model four gravity waves in airglow emissions as observed from the ground to numerically predict whether these waves could have been observed from space. In spite of encountering critical levels, some waves may still be observed in the airglow provided the critical level lies within the airglow emission region. One of the four waves experiences a critical level in the lower region of an airglow layer such that the disturbance to the volume emission rate would be effectively limited to a short distance along a satellite line of sight. The effect of this is to mitigate the effects of destructive interference in the airglow making the wave more observable from space. For this particular wave the amplitude is derived by normalizing the model-derived airglow fluctuation amplitude to that observed from the ground during the ALOHA-93 campaign. The model then provides momentum and energy fluxes as a function of height as well as the flux divergences, from which the mean state forcing is evaluated. The results suggest that the observed wave could provide significant mean state forcing. Therefore, we conclude that some waves experiencing critical level interactions in the airglow regions are not only likely to be important to the momentum balance of the upper mesosphere/lower thermosphere region but also are more likely to be observed from space. *INDEX TERMS:* 3384 Meteorology and Atmospheric Dynamics: Waves and tides; 3334 Meteorology and Atmospheric Dynamics: Middle atmosphere dynamics (0341, 0342); 0310 Atmospheric Composition and Structure: Airglow and aurora; 3367 Meteorology and Atmospheric Dynamics: Theoretical modeling; *KEYWORDS:* gravity waves, airglow, satellite observations, simulations

Citation: Hickey, M. P., and J. S. Brown, A simulation study of space-based observations of gravity waves in the airglow using observed ALOHA-93 wave parameters, *J. Geophys. Res.*, *107*(A12), 1431, doi:10.1029/2001JA009225, 2002.

1. Introduction

[2] Satellite measurements of atmospheric gravity wave disturbances in mesospheric airglow emissions suffer from an inherent 180° ambiguity in horizontal phase propagation direction due to the fact that the wave system appears stationary to a fast moving satellite. However, *Hickey and Brown* [2000] and *Brown and Hickey* [2001] have recently performed numerical simulations that demonstrate the feasibility of removing the 180° ambiguity associated with space-based measurements for gravity waves of short vertical wavelength. Serendipitously, the short vertical wavelength waves are those waves expected to be important to the mesopause region momentum budget, because they will be subject to strong damping or nonlinear effects. The 180° ambiguity in propagation direction cannot be easily removed for waves of larger vertical wavelength, but these waves will usually propagate to much higher altitudes before dissipating or breaking, and so are not usually expected to be important to the momentum budget of the mesopause region.

[3] The simulations described by *Hickey and Brown* [2000] and *Brown and Hickey* [2001] used a full-wave model describing gravity wave propagation subject to the effects of the eddy and molecular diffusion of heat and momentum and the Coriolis force. Wind effects that are usually included in the model [e.g., *Hickey et al.*, 1997, 1998] were not included in these two more recent studies. However, winds significantly affect gravity wave propagation through the atmosphere, especially in the mesopause region where they can be significant [e.g., *Larsen*, 2000, 2002]. In some instances waves can encounter critical levels, impeding their propagation to greater altitudes [e.g., *Taylor et al.*, 1993].

[4] During the ALOHA-93 campaign (Hawaii, 20.8°N, 156.2°W), many gravity wave events were recorded in the mesospheric nightglow emissions [*Taylor et al.*, 1995; *Swenson et al.*, 1995; *Hecht et al.*, 1995]. The wave observations using airglow-imaging systems were often accompanied by lidar observations of winds and temperatures [*Gardner et al.*, 1995; *Tao and Gardner*, 1995]. The combination of fairly extensive sets of wave parameters and

[1]Now at Department of Physical Sciences, Embry-Riddle Aeronautical University, Daytona Beach, Florida, USA.

0148-0227/02/2001JA009225

a good description of the mean horizontal winds in the airglow regions prompted *Hickey et al.* [1998] to model the airglow response to the waves. A feature revealed by this modeling was that occasionally gravity waves encountered critical levels in the airglow region. In one particular case it was shown that an observed wave had a critical level lying within the OI 5577 airglow emission region below the altitude of the peak volume emission rate (VER), demonstrating that sometimes waves can be observed in the airglow despite their critical level encounters within the airglow emission regions. This can occur because it allows some portion of the wave to produce a significant perturbation to the altitude integrated VER [*Hickey et al.*, 1998].

[5] It is accepted that in order for gravity waves to be observed from the ground, their associated VER perturbations must survive integration along the line of sight over the vertical extent of the emission region. For the same waves to also be observed in space-based observations requires that the wave associated VER fluctuations survive integration along a tangent ray. The complicating effects of winds, and especially the existence of critical levels, makes the prediction of observing a wave from space given its observation from the ground almost impossible. While it appears from our previous ALOHA simulations that ground-based observations may detect waves in the airglow that encounter such critical levels, it is not known whether space-based observations could detect these same waves. In particular, it is not obvious that waves of short vertical wavelength observed from the ground could also be observed from space in the presence of realistic background winds.

[6] The purpose of this paper is to perform a modeling study to determine whether or not certain simulated waves can be simultaneously observed from the ground and from space when wind effects are included in the analysis. In particular, we will simulate waves that were actually observed from the ground during the ALOHA-93 campaign. To do so, we will use the wave parameters derived from the airglow imager observations described by *Hickey et al.* [1998]. We will also use the winds derived from the observations of *Gardner et al.* [1995] and *Tao and Gardner* [1995] during ALOHA-93 that were colocated in time and space with the wave measurements. Brightness fluctuations in the OI 5577 nightglow emission and the O_2 atmospheric nightglow emission will be simulated. As will be shown, of the four different waves observed from the ground, our simulations suggest that only one could be observed from space for the prevailing conditions at the time of the observations. We also calculate the vertical profile of the energy flux, the momentum flux, and the associated mean state forcing associated with the dissipation of the four waves.

2. Method

2.1. Model Description

[7] The full-wave model that forms the basis for these calculations has been described extensively elsewhere [*Hickey et al.*, 1997, 1998, 2000]. Briefly, it is a linear, steady state model that solves the Navier-Stokes equations for wave propagation in a nonisothermal background atmosphere including height-dependent mean winds, and includes the Coriolis force and the eddy and molecular diffusion of heat and momentum. The nominal eddy diffusion profile approximates that presented by *Strobel* [1989], with a nominal maximum value of 100 m^2 s^{-1} occurring at 90 km altitude. With the mean, undisturbed atmosphere defined, the model requires input of wave period, horizontal wavelength, and azimuth of propagation. The model output includes height profiles of wave amplitudes and phases for the temperature and pressure fluctuations and the horizontal and vertical velocity fluctuations. These are then input to a steady state chemistry model describing the response of chemical minor species to gravity waves, from which fluctuations in airglow VER are calculated as a function of height. Integration of the VER fluctuations over altitude provides a simulation of ground-based observations of airglow brightness fluctuations due to gravity waves, as described in *Hickey et al.* [1998] and references therein. In order to simulate space-based observations of gravity wave-driven airglow fluctuations the fluctuation VER is integrated along a chosen line of sight, which can include those associated with sublimb observations [*Hickey and Brown*, 2000; *Brown and Hickey*, 2001].

2.2. Mean Wind Profiles

[8] In this study we simulate wave propagation in our model using winds derived from lidar measurements obtained during the ALOHA-93 campaign. Our approach is similar to that of *Hickey et al.* [1998] except in two respects. First, instead of using an analytic function to represent these measured winds (see *Hickey et al.* [1998] for a description of this), we instead use a smoothing spline to fit these data. We have found that the latter approach is a superior method, as described in the next section. Second, our derived smoothing spline is not constrained to fit every data value, but is instead chosen to represent the larger vertical scale tidal structure. Smaller-scale structure associated with gravity waves is therefore precluded from our description of the mean winds. This is a reasonable approach because we are interested in how gravity waves perturb the mean state, and the mean should not include such waves.

[9] We find that, in general, the measured meridional winds are large ($\sim$100 m s^{-1}) below 85 km altitude. In order to determine the sensitivity of our wave simulations to these large mean meridional winds we use a second set of meridional wind profiles that are $\sim$60% of the nominal meridional winds for the night of 21 October. The zonal winds are not large at low altitudes, but they can achieve large values at higher altitudes ($\sim$100 km). Therefore they should not significantly influence wave effects at lower altitudes in the airglow region, and so we do not perform a similar sensitivity test for the zonal winds. The wind data exists for altitudes between about 80 km and 105 km altitude. Our smoothing spline fit is tailored to ensure that at both low and high altitudes the winds smoothly approach zero for both the meridional and zonal winds.

[10] The mean winds for the nights of 7, 20, and 21 October 1993 are shown in Figures 1a, 1b, and 1c, respectively. On the night of 7 October the meridional wind (solid curve) achieves a maximum northward value of $\sim$45 m s^{-1} near 90 km and 102.5 km altitude and a maximum southward value of $\sim$40 m s^{-1} near 83 km and 98 km altitude.

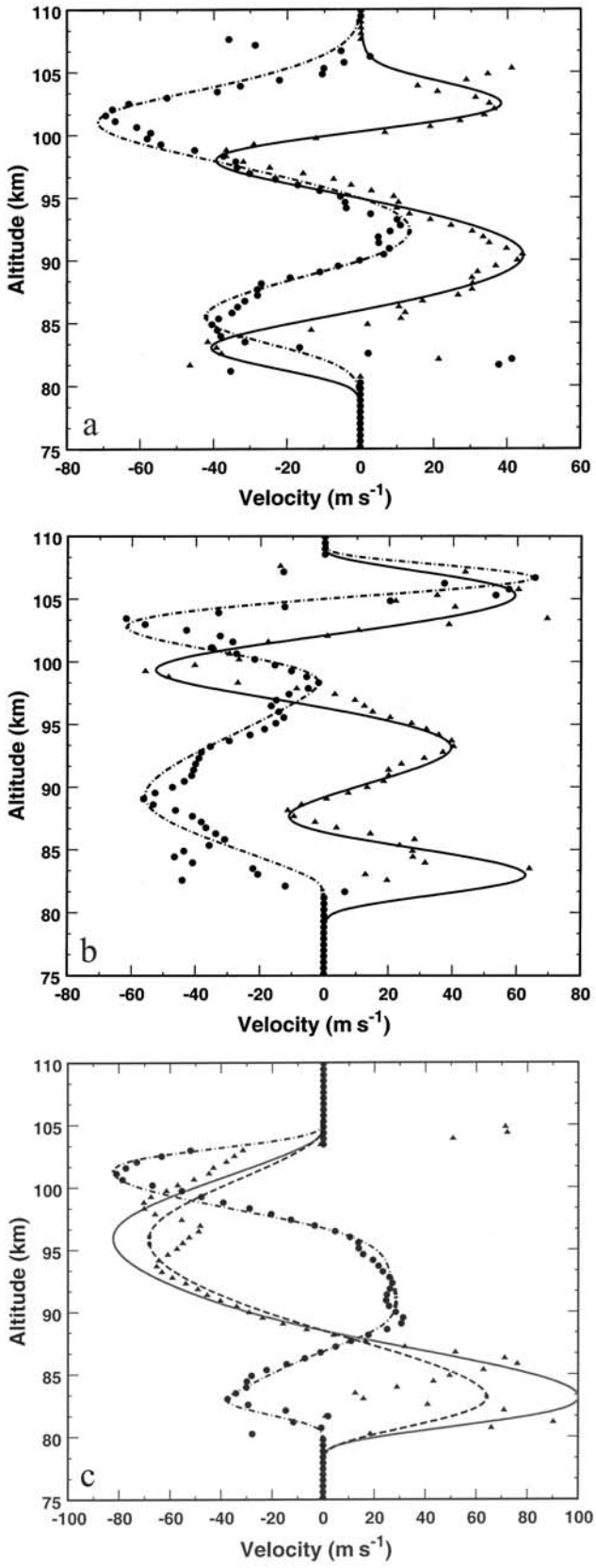

Maximum zonal winds (dashed-dotted curve) are ~15 m s^{-1} eastward (near 92 km altitude) and 70 m s^{-1} westward (near 101 km altitude). On the night of 20 October the meridional wind (solid curve) achieves a maximum northward value of ~62 m s^{-1} near 83 km altitude and a maximum southward value of ~55 m s^{-1} near 99 km altitude. Maximum zonal winds (dashed-dotted curve) are 57 m s^{-1} and 62 m s^{-1} westward near 89 and 102.5 km altitude, and the maximum eastward wind (~66 m s^{-1}) occurs near 107 km altitude. On the night of 21 October the nominal meridional wind (solid curve) achieves maximum northward values of ~100 m s^{-1} near 83 km altitude, and maximum southward values of ~80 m s^{-1} near 96 km altitude. The second meridional wind profile (dashed curve) has winds that are ~60% of the nominal meridional wind profile values near local extrema, and is used as a sensitivity test for these winds. The zonal wind profile (dashed-dotted curve) is characterized by small westward winds below about 86 km altitude, eastward winds of ~25 m s^{-1} between 90 and 95 km altitude, and westward winds above 96 km altitude, reaching a maximum westward value of ~80 m s^{-1} near 101 km altitude.

3. Results

3.1. Comparison of the Four Waves

[11] Simulations are performed using the four sets of wave parameters provided in Table 1. These are the same wave parameters used in the study of *Hickey et al.* [1998]. All of the waves have a dominant southward direction of propagation except for wave D, which propagates southwest. The waves are characterized by fairly short extrinsic wave periods (≤10 min), modest horizontal phase trace speeds (≤53 m s^{-1}), and relative brightness fluctuation amplitudes in the OI 5577 nightglow emission ranging from 3% to 6.7%. Three of the waves encounter critical levels, which occur at altitudes where the background wind velocity equals the phase velocity. Critical levels exist near 98.9 km, 93.9 km, and 95.4 km for waves B, C and D, respectively. Although wave A does not encounter a critical level, in agreement with the results of *Hickey et al.* [1998], its intrinsic phase speed becomes small near 82.65 km altitude.

[12] Using the MSIS model [*Hedin*, 1991] to define the basic undisturbed state (major gas densities and temperature, as well as O number density), and using the chemical rate constants given by *Hickey and Walterscheid* [1999], we derive the VER for the OI 5577 and O_2 atmospheric airglow emissions. The O_2 atmospheric VER (not shown) peaks just below 91.5 km altitude with a value of ~3.75 × 10^8 photons m^{-3} s^{-1}. The OI 5577 VER (not shown) peaks near 95 km altitude with a value of ~4.0 × 10^8 photons

Figure 1. (opposite) Mean meridional wind data (filled triangles) and smooth fit (solid curves, positive due north) and zonal wind data (filled circles) and smooth fit (dashed-dotted curves, positive due east) for the nights of (a) 7 October, (b) 20 October, and (c) 21 October 1993. For the night of 21 October only, a second meridional wind profile (dashed curve) is also shown with values that are ~60% of the nominal values.

Table 1. Observed Wave Parameters Derived From a Spectral Analysis of the OI (557.7 nm) Image Data and Estimates of the Wave Amplitude Ratios on 7, 20, and 21 October 1993 [after *Hickey et al.*, 1998]

	λ_h, km	Period, min	Azimuth, deg	V_{ph}, m s^{-1}	$\langle \delta I \rangle / \langle \bar{I} \rangle$	Contrast, %
Wave A 7 October 1993	20.0	9.0	150.0	37.0	4.6 ± 0.6	9.2 ± 1.2
Wave B 20 October 1993	28.6	9.5	180.0	50.2	6.7 ± 0.6	13.4 ± 1.2
Wave C 21 October 1993	30.1	9.5	210.0	52.8	5.7 ± 0.6	11.4 ± 1.2
Wave D 21 October 1993	19.9	10.2	235.0	32.5	3.0 ± 0.6	6.0 ± 1.2

m^{-3} s^{-1}. The thickness of each of the two airglow layers (defined as the full-width at half-maximum) is ~8 km.

[13] Following the procedure derived by *Hickey et al.* [1998], simulated ground-based airglow fluctuation amplitudes derived from the full-wave model are scaled to match those observed. The resulting temperature perturbation amplitudes (T') for all four waves are shown as a function of altitude in Figure 2a. The maximum values of T' occurring in the airglow region obtained here are at least a factor of two smaller than those obtained previously by *Hickey et al.* [1998]. There are two reasons for this difference. First, by not including small vertical-scale structure in the winds we are now using a smoother altitude profile of the mean winds than used previously. This tends to reduce the local gradients of the mean winds, which reduces wave reflection. Second, we now employ a far superior method, using a smoothing spline, to fit these winds. The previous analytic fit did not ensure continuity of the second derivative of wind with respect to altitude (d^2u/dz^2). Discontinuities in d^2u/dz^2 will always lead to an increase in wave reflection in the full-wave model and to smaller wave amplitudes in the airglow region. The rescaling of T' required to achieve the desired (observed) value of the relative airglow brightness fluctuation amplitude $B'/\bar{B}$ then produces final values of T' that are larger than those obtained using the smoothing splines. Maximum values of T' in the 90–100 km region are now about 5 K, 1.7 K, 12 K, and 1.2 K for waves A, B, C and D, respectively. The effects of wave reflection are evident as amplitude undulations over altitude in all four profiles.

[14] The phases of the temperature perturbations ($\varphi(T')$) for the four waves are shown in Figure 2b. Throughout much of the airglow region (90–100 km altitude) the vertical wavelengths of waves A and B are relatively large (≥15 km and ≥7 km, respectively), while those of waves C and D are relatively small (1–2 km and 2–3 km, respectively). For wave C, the small vertical wavelengths begin to occur in regions below the critical level (near 93.8 km altitude for the nominal winds), whereas for wave D the small vertical wavelengths begin to occur in regions very near the critical level (near 95.4 km altitude). Therefore, increased cancellation between VER fluctuations occurring at different altitudes associated with small vertical wavelengths occurs mainly for wave C. Wave D amplitudes and associated VER fluctuation amplitudes are too small in the region where small vertical wavelengths occur to significantly impact the height-integrated VER (or brightness) fluctuation. Cancellation effects in the airglow are minimal for waves A and B.

[15] As previously found by *Hickey and Brown* [2000] and *Brown and Hickey* [2001], we find that for all of our space-based simulations the relative brightness fluctuations are always larger when viewing normal to the gravity wave phase fronts in the backward direction compared to the forward direction (for a satellite and wave system moving in the same direction). Therefore, in order to determine which of those waves observed from the ground could also be observed from space we perform additional simulations of space-based observations of these waves using the method

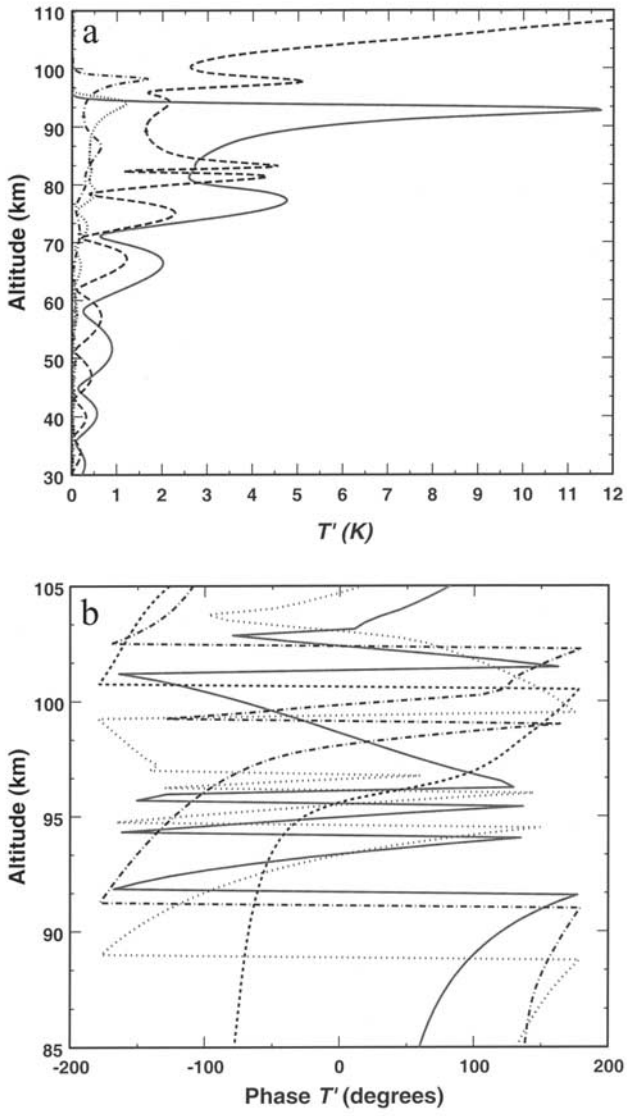

Figure 2. Altitude profile of derived wave temperature perturbation (a) amplitudes and (b) phases that give the desired airglow fluctuation amplitude for wave A (dashed curve), wave B (dashed-dotted curve), wave C (solid curve), and wave D (dotted curve).

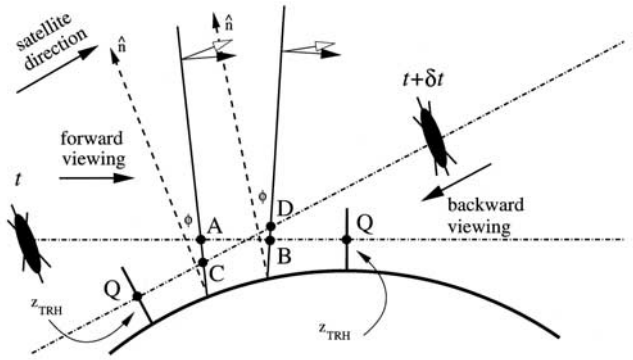

Figure 3. Schematic (not to scale) representing the difference associated with viewing direction of an airglow disturbance. The solid lines represent lines of constant phase at angle φ relative to a local vertical coordinate (dashed lines). Arrows represent the total (solid) and horizontal (open) wave number vectors. The dash-dotted lines represent the tangent ray paths for forward (at time t) and backward (at time $t + \delta t$) viewing for a given tangent ray height z_{TRH}. The apparent wavelengths represented by the distances $\overline{AB}$ (for forward viewing) and $\overline{CD}$ (backward viewing) are not equal ($\overline{CD} > \overline{AB}$), leading to increased destructive interference and a smaller brightness fluctuation for forward viewing. [After *Brown and Hickey*, 2001].

discussed by *Hickey and Brown* [2000] and *Brown and Hickey* [2001]. The geometry relevant to the observation of a gravity wave perturbation of the airglow VER as observed from a space-based instrument has been provided previously by *Hickey and Brown* [2000] and *Brown and Hickey* [2001], and is shown here in Figure 3. The details of this modeling are not repeated here but can be found in our previous work.

[16] In Table 2 we compare the results obtained for ground-based and space-based simulations of airglow relative brightness fluctuations, the latter derived for backward viewing. We do so for the OI 5577 and O_2 atmospheric (0–0 and 0–1 band) nightglow emissions. The values of $B'/\bar{B}$ for ground-based viewing and for the OI 5577 nightglow are those values used by *Hickey et al.* [1998]. The ground-based values of $B'/\bar{B}$ for the O_2 atmospheric nightglow (column 3 of Table 2) pertain to our simulations of the 0–1 band of this system. These results suggest that waves A and C would produce stronger fluctuations in the O_2 atmospheric nightglow than in the OI 5577 nightglow, whereas for waves B and D the reverse is true. However, no observations of the O_2 atmospheric nightglow were available for comparison at the time of the OI 5577 nightglow observations.

Table 2. Summary of Ground-Based and Space-Based Backward Viewing Simulations of the Relative Brightness Fluctuations for the Wave Parameters Provided in Table 1 Using the Nominal Winds

Wave	Emission	$B'/\bar{B}$ Ground, %	$B'/\bar{B}$ Space, %	$B'/\bar{B}$ Space 0–0 Band, %
A	OI 5577	4.60	0.08	-
	O_2 Atm.	6.30	0.03	0.07
B	OI 5577	6.70	0.95	-
	O_2 Atm.	1.60	0.16	0.17
C	OI 5577	5.70	5.30	-
	O_2 Atm.	7.80	2.20	4.50
D	OI 5577	3.00	1.50	-
	O_2 Atm.	0.76	0.29	0.65

[17] Column 4 of Table 2 provides values of $B'/\bar{B}$ for the OI 5577 and O_2 atmospheric 0–1 band for space-based viewing, while column 5 shows values of $B'/\bar{B}$ for the O_2 atmospheric 0–0 band for space-based viewing. For wave C space-based values of $B'/\bar{B}$ are slightly smaller than the corresponding ground-based values, and the largest values occur for the OI 5577 nightglow emission (5.3% for space-based versus 5.7% for ground-based). The largest value of $B'/\bar{B}$ for wave C and for the O_2 atmospheric nightglow occurs for the 0–0 band nightglow emission (4.5%). Although for wave D the space-based value of $B'/\bar{B}$ for the O_2 atmospheric nightglow 0–0 band emission (0.65%) is comparable to the ground-based value of $B'/\bar{B}$ for the 0–1 band (0.76%), both values are small and are presumably below the detection limit. Wave A was observed from the ground in the OI 5577 nightglow (see Table 1). However, while these results suggest that it could also have been observed from the ground in the O_2 atmospheric 0–1 band nightglow (see column 3), they also demonstrate that it would not have been observable from space (see columns 4 and 5). Wave B was also observed from the ground in the OI 5577 nightglow. The results suggest that this wave would not be easily detected in ground-based observations of the O_2 atmospheric 0–1 band nightglow, and that it would be unobservable from space.

[18] The space-based simulation results can best be understood by examination of the VER fluctuations along the line of sight. We first present a schematic depicting two waves propagating upward through an airglow emission layer (Figure 4). A space-based instrument observes the airglow along a line of sight having a tangent ray point that lies well below the height of the airglow layer. One of the waves propagates through the entire vertical extent of the layer, while the second wave does not because it encounters

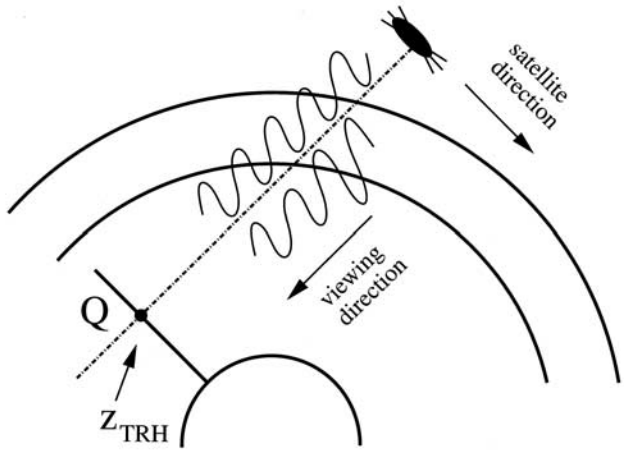

Figure 4. Schematic depicting two waves propagating upward through an airglow emission layer, with one wave encountering a critical level within the airglow emission layer.

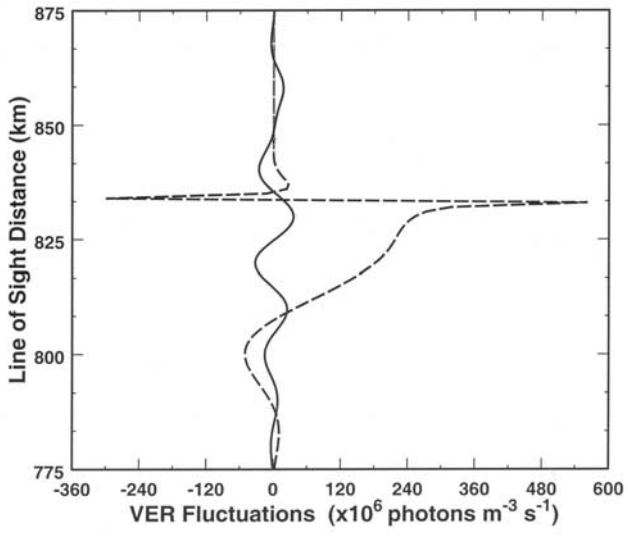

Figure 5. VER fluctuations plotted as a function of distance along the line of sight for backward viewing in the OI 5577 nightglow for waves A (solid curve) and C (dashed curve).

a critical level within the layer. Consequently, VER fluctuations will extend further along the line of sight for the former wave. In Figure 5 we present the line of sight VER fluctuations for waves A and C and for backward viewing in the OI 5577 airglow emission. For wave A several VER fluctuations occur along the line of sight through the emission layer. Therefore, when the VER fluctuations are integrated along the line of sight to simulate the observed airglow brightness, significant cancellation occurs and the simulated values of $B'/\bar{B}$ are consequently small. For wave C the VER fluctuations occur over a limited extent along the line of sight, and the apparent wavelength is quite large (there is less than one complete fluctuation). Therefore, cancellation effects are minimal in the line of sight integration of the VER fluctuations, and simulated values of $B'/\bar{B}$ are significant. The result of this is that wave C would be observable from space whereas wave A would not. The results for waves B and D are similar to those of wave A and so are not shown. Likewise, the results for the O_2 atmospheric airglow emission are not shown because they appear similar to those presented here for the OI 5577 airglow emission.

3.2. Simulations for Wave C

[19] The results of our simulations summarized in Table 2 suggest that of all four waves, only wave C would be likely to be observed simultaneously from the ground and space were such simultaneous measurements available. The sensitivity of these results to the winds is examined by either reducing the magnitude of the meridional winds to ~60% of their nominal values in regions of maximum winds, or by setting the meridional and zonal winds to zero at all altitudes (i.e., ignoring wind effects). In both of these separate cases, the wave simulations were performed based on the requirement that the temperature perturbation amplitude (T') at a low altitude (~37 km) be equal to that used in the nominal simulation at the same altitude. The rationale for this is that a given lower atmospheric gravity wave source (perhaps at ~10 km altitude) will produce waves of amplitudes that are independent of the high altitude (≥50 km) winds.

[20] After performing these sensitivity tests we found that three of the waves (A, B and D) had small space-based values of $B'/\bar{B}$ (much less than 1%) in all cases, and so they are not considered further in our analysis except in section 3.4. Our sensitivity tests revealed that of the four waves considered only wave C could be observed from space. Results for wave C are summarized in Table 3. The nominal results for wave C that appeared in Table 2 are repeated in Table 3 for comparison purposes. When the effects of mean winds are ignored ground-based values of $B'/\bar{B}$ significantly exceed their nominal values. This is because wave amplitude (not shown) grows with increasing altitude at a faster rate in the absence of winds (for these particular simulations). When the ~60% nominal meridional winds are included the maximum value of T' (not shown) is smaller (~6.3 K) and occurs about 1 km higher than the nominal maximum value of T'(~11.8 K). However, we have set the values of T' to be equal at 37 km altitude in these two different wind cases, and at this altitude a node occurs in T' associated with wave reflection. The fact that the reflection appears to be stronger in the nominal wind case, as inferred from the larger amplitude excursions between nodes and antinodes, means that the wave amplitudes at the antinodes are greater in the case of the nominal mean winds. Therefore, we are most probably underestimating the wave energy flux when we use the ~60% nominal meridional winds. This will not adversely affect our results and conclusions, however, because it implies that we are using conservative estimates of wave amplitude for wave C by using the nominal mean winds. Wave amplitudes could be larger than those discussed here for the case of the ~60% nominal meridional winds.

[21] The vertical wavelength in the airglow emission region (not shown) is much greater in the windless case, which decreases the effects of interference in VER fluctuations occurring at different altitudes, thereby producing larger values of $B'/\bar{B}$. However, the space-based values of $B'/\bar{B}$ are significantly smaller than the respective nominal values. This is because in the absence of winds the waves propagate through the entire vertical extent of the airglow emission layer. Therefore, for space-based viewing, significant VER fluctuations occur over a significant length along the line of sight. As previously discussed in relation to the results presented in Figure 2, this leads to significant cancellation between VER fluctuations occurring at different positions, and hence small values of $B'/\bar{B}$. The use of

Table 3. Sensitivity of Wave C Results to Winds for Ground-Based and Space-Based Backward Viewing

Winds	Emission	$B'/\bar{B}$ Ground, %	$B'/\bar{B}$ Space, %	$B'/\bar{B}$ Space 0–0 Band, %
Nominal	OI 5577	5.70	5.30	-
	O_2 Atm.	7.80	2.20	4.50
None	OI 5577	23.00	<0.01	-
	O_2 Atm.	19.00	0.02	0.03
60% Nominal	OI 5577	5.70	4.60	-
	O_2 Atm.	5.00	1.00	2.10

meridional winds that are ~60% of the nominal values has a relatively small effect on ground-based values of $B'/\bar{B}$. Although the space-based values of $B'/\bar{B}$ are reduced over their nominal values in this case, the waves would still be observed in the OI 5577 nightglow emission for which $B'/\bar{B}$ is about 4.6%. The critical level lies at a higher altitude (~95 km) in the case of the smaller (~60% nominal) winds compared to the critical level altitude of ~93.9 km for the nominal winds. Therefore, although the gravity wave propagates upward through most of the vertical extent of the O_2 atmospheric emission layer, it does not propagate completely through the OI 5577 emission layer. It is this fact, as well as the fact that the vertical wavelength is $\leq$2 km throughout much of the O_2 atmospheric airglow region, that allows the wave to be more easily observed from space in the OI 5577 airglow emission than in the O_2 atmospheric airglow emission.

[22] Values of $B'/\bar{B}$ for space-based simulations of the OI 5577 and O_2 atmospheric 0–0 and 0–1 band nightglow emissions are presented in Table 4, and results obtained for forward and backward viewing are compared. For the OI 5577 emission $B'/\bar{B}$ is about a factor of 2 greater for backward viewing compared to forward viewing (for a satellite and wave moving in the same direction). This difference arises due to the geometry effects discussed by *Hickey and Brown* [2000] and *Brown and Hickey* [2001], wherein the apparent wavelength in the airglow is shorter for forward viewing (that is, for viewing from "behind" the wave). Figure 6 shows VER fluctuations for wave C and the nominal winds, and for both forward and backward viewing, and for the O_2 atmospheric and OI 5577 airglow emissions. For both the OI 5577 and O_2 atmospheric emissions, the apparent wavelength in the VER fluctuations is significantly smaller for forward viewing, producing more cancellation and smaller values of $B'/\bar{B}$. Values of $B'/\bar{B}$ obtained for the O_2 atmospheric 0–1 band emission are not large (~1% for forward viewing and ~2% for backward viewing), meaning that the wave would not be easily observed. However, for the 0–0 band of the O_2 atmospheric emission, the value of $B'/\bar{B}$ for backward viewing is 4.5% and large enough to be observed. For forward viewing $B'/\bar{B}$ is less than half this value (2.1%). Therefore, these results suggest that direction of wave propagation could be determined from space-based observations of either the OI 5577 nightglow or of the 0–0 band of the O_2 atmospheric nightglow.

3.3. Smearing Effects for Wave C

[23] We have simulated the effects of smearing associated with the finite time for an instrument to make a measurement with a good signal-to-noise ratio using the approach discussed by *Brown and Hickey* [2001]. We considered only the OI 5577 nightglow emission for backward viewing. The value of $B'/\bar{B}$ was reduced from its nominal value of 5.7% to 5.2% and 5.0% for smearing times of 0.5 and 1.0 s, respectively. These values suggest that wave C would be observable provided instrument-averaging times do not exceed ~1 s. This is not an unreasonable smearing time based on current technology, as discussed in detail in *Brown and Hickey* [2001]. Larger smearing times of ~2.5 s or more would render this wave unobservable.

Table 4. Comparison of Relative Brightness Fluctuations (in %) for Wave C for Space-Based Simulations of Forward and Backward Viewing Using the Nominal Winds

Emission	$B'/\bar{B}$: Thin Forward	$B'/\bar{B}$: Thin Backward	$B'/\bar{B}$: Thick Forward	$B'/\bar{B}$ Thick Backward
OI 5577	2.80	5.30	-	-
O_2 Atm.	1.10	2.20	2.10	4.50

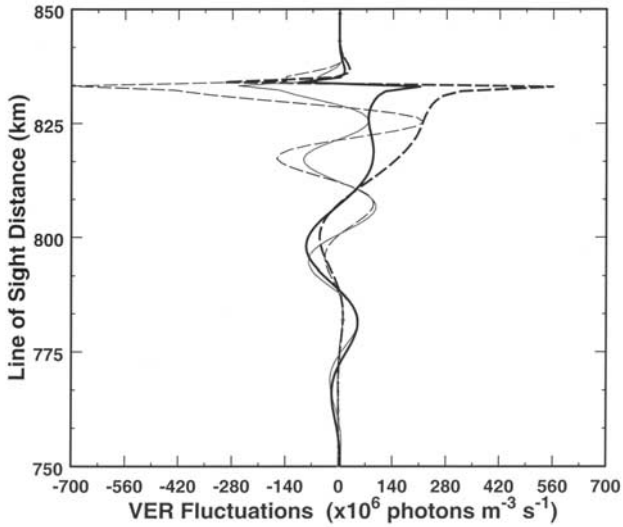

Figure 6. VER fluctuations for wave C plotted as a function of distance along the line of sight for backward (thick solid curve) and forward (thin solid curve) viewing in the O_2 atmospheric airglow, and for backward (thick dashed curve) and forward (thin dashed curve) viewing in the OI 5577 nightglow.

3.4. Wave Action, Momentum Fluxes, and Momentum Forcing for Wave C

[24] In an atmosphere free of dissipation and with height-varying mean winds, the wave energy flux is no longer conserved [*Bretherton and Garrett*, 1968], whereas the wave action, defined as $(\omega/\Omega)\langle w'p'\rangle$ (where $\Omega = \omega - k \cdot \bar{U}$ is the intrinsic wave frequency and $\bar{U}$ is the mean horizontal wind) is conserved. An alternative form of the wave action [*Lindzen*, 1990] is calculated in the full-wave model:

$$F_E = \langle w'p'\rangle + \bar{\rho}\,\bar{U}\,\langle u'\,w'\rangle + \bar{\rho}\,\bar{V}\,\langle v'\,w'\rangle. \quad (1)$$

Here, $\bar{\rho}$ is the mean atmospheric density, $\bar{U}(\bar{V})$ is the mean meridional (zonal) wind, u', v', and w' are the perturbation meridional, zonal, and vertical wind, respectively, and the angle brackets denote averaging over one wave period and one horizontal wavelength. The wave action is not conserved when waves are dissipated. Because wave dissipation due to diffusion in our model (the eddy diffusion has a maximum value of 100 $m^2\ s^{-1}$ at 90 km altitude) is scale-dependent, it increases near critical levels where the vertical wavelength becomes small. Therefore, the wave action is particularly not conserved at critical levels.

[25] We plot F_E as a function of height for the four waves propagating through the nominal mean winds (see

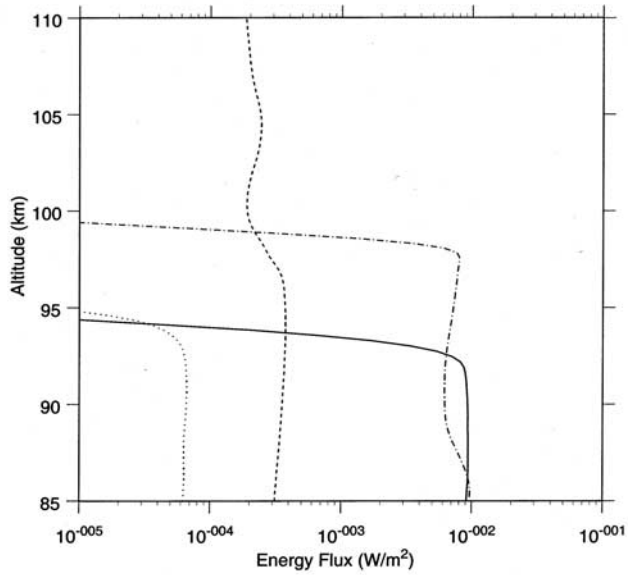

Figure 7. Vertical energy flux plotted as a function of height for waves A (dashed curve), B (dashed-dotted curve), C (solid curve), and D (dotted curve) propagating through the nominal mean winds.

Figure 7). For wave C and below about 92 km altitude F_E is constant, as expected for a nondissipative wave, and equal to $\sim 10^{-2}$ W m^{-2}. However, as wave C approaches the critical level (which is located at ~93.9 km altitude) its intrinsic phase speed is reduced and it begins to dissipate. The Richardson number (*Ri*, not shown) exceeds unity in the vicinity of the critical level ($Ri \approx 10$), indicating a broad critical region and consequently severe attenuation as the wave propagates through it [*Breeding*, 1971]. The energy flux associated with wave C is reduced by a factor of ~100 between about 92 km and 94 km altitude. The energy fluxes of waves B and D are similarly substantially reduced after propagation through their respective critical levels. Below about 92 km altitude the energy fluxes for waves A and D are considerably smaller than the energy flux for wave C (by factors of about 30 and 100, respectively). The energy flux of wave B is comparable to, but slightly less than that of wave C throughout most of the airglow region. However, whereas the energy flux of wave C decreases rapidly above about 94 km altitude, the rapid decrease of energy flux occurs above about 99 km altitude for wave B because its critical level lies at a higher altitude. Wave A does not encounter a critical level in the airglow region, and so compared to the other waves a substantial energy flux reaches altitudes above the airglow region.

[26] The meridional and zonal velocity perturbations (not shown) for wave C propagating in the nominal mean winds maximize near 92.5 km altitude with values of ~29 m s^{-1} and ~16 m s^{-1}, respectively. The vertical velocity perturbation maximizes several kilometers lower near 86 km altitude, with a value of ~8.7 m s^{-1}. Phase differences between the horizontal and vertical velocity fluctuations (not shown) are relatively small (<10°) over much of the altitude range of interest.

[27] Figure 8 shows the zonal and meridional momentum fluxes per unit mass ($\langle u'w' \rangle$ and $\langle v'w' \rangle$, respectively) for wave C plotted as a function of height. The fluxes in the zonal and meridional directions vary with altitude in a similar manner, achieving maximum values near 92 km altitude, and decreasing rapidly with increasing height at higher altitudes as a consequence of the critical level interaction. Maximum momentum fluxes per unit mass are ~53 m^2 s^{-2} and ~−33 m^2 s^{-2} for the meridional and zonal directions, respectively. The corresponding maximum momentum fluxes per unit mass for waves B and D (not shown) are small by comparison ($\leq$4 m^2 s^{-1}). In the case of wave A, the maximum momentum flux per unit mass (not shown) is fairly small ($\leq$10 m^2 s^{-1}) in the airglow region. Above the airglow region, the wave amplitude grows and so too does its momentum flux per unit mass (not shown), achieving a maximum value in the meridional direction of ~65 m^2 s^{-2}. However, these large values of momentum flux per unit mass for wave A occur in a region where the mean winds have been forced to approach small (and unrealistic) values because this region is above our primary region of interest.

[28] The magnitude of the momentum flux per unit mass for wave C is ~64 m^2 s^{-2}. This value is significantly smaller than the ~900 m^2 s^{-2} inferred from recent observations of a wave disturbance in the airglow [*Fritts et al.*, 2002]. The observed wave parameters in their study (horizontal wavelength ~27 km and period ~5.6 min) are similar to those of wave C. The larger wave amplitudes of 50 m s^{-1} and 35 m s^{-1} for the horizontal and vertical velocity perturbations, respectively, employed by *Fritts et al.* [2002] can account for some of the difference between the values of momentum fluxes per unit mass given above. Our maximum horizontal and vertical velocity perturbation amplitudes are ~29 m s^{-1} and 16 m s^{-1}, respectively.

[29] Associated with the dissipation of gravity waves is momentum forcing of the mean state associated with a

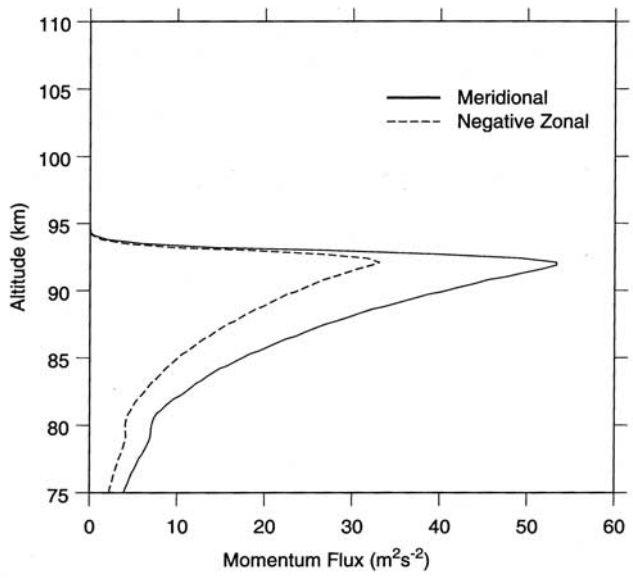

Figure 8. Meridional (solid curve) and zonal (dashed curve) momentum fluxes per unit mass plotted as a function of height for wave C propagating through the nominal mean winds.

violation of the nonacceleration conditions [*Eliassen and Palm*, 1961; *Andrews and McIntyre*, 1976; *Fritts*, 1984]. For wave C we calculate the mean state acceleration in the meridional direction using the expression $d\bar{U}/dt = -(1/1\bar{\rho})\, d(\bar{\rho}\langle u'w'\rangle)/dz$. A similar expression with v' replacing u' is used to calculate the mean state acceleration in the zonal direction. Figure 9 shows the zonal and meridional acceleration, in units of m s^{-1} hr^{-1}, for the case of nominal winds. Accelerations are large for this wave ($\sim$120 m s^{-1} hr^{-1} and 200 m s^{-1} hr^{-1} in the zonal and meridional directions, respectively) due to the existence of a strong critical level. The magnitude of the acceleration is $\sim$230 m s^{-1} hr^{-1}. (The acceleration derived using the $\sim$60% nominal meridional winds (not shown) occurs about 1 km higher than those for the nominal winds with a smaller magnitude.) Using airglow observations *Fritts et al.* [2002] inferred a mean state change in velocity of $\sim$80 m s^{-1} over a region of atmosphere one scale-height thick for a gravity wave forcing duration of $\sim$10 min. This equates to very large forcing ($\sim$500 m s^{-1} hr^{-1}), that is nonetheless comparable to our value given above. Although these accelerations are large, they will generally occur for relatively short periods of time over fairly localized regions of the atmosphere with the result that zonal-mean accelerations would be much smaller. It is interesting to note that this wave was observed for a few hours during the ALOHA-93 campaign [M. J. Taylor, private communication, 2001], suggesting that the local mean state acceleration could have been very large. Perhaps related to this, *Zhu et al.* [1997] have used a globally balanced 2-D model and found that large accelerations induced by gravity wave drag were required to produce a mean temperature distribution in agreement with observed meridional mean temperature gradients. Their inferred zonal-mean accelerations were large in the midlatitude summer mesopause region (400 m s^{-1} day^{-1}).

[30] Thus, waves for which the 180° ambiguity in direction of propagation can be determined from space will usually have short vertical wavelengths in the airglow region (90–100 km altitude) and will usually be strongly dissipated. As noted by *Hickey and Brown* [2000] and *Brown and Hickey* [2001], it is serendipitous that waves whose direction can be determined from airglow observations are also those waves most likely to produce significant forcing of the mean state in the airglow region. We realize that our steady state model must overestimate this forcing. Intermittence and spatial localization must be taken into account when considering wave sources in the atmosphere. Therefore, accelerations of this magnitude could not persist for extended periods of times, and time-dependent modeling would be required to evaluate the time evolution of the mean state.

4. Discussion

[31] Many of the caveats associated with our simulations as they relate to space-based observations have been discussed extensively in *Brown and Hickey* [2001] and will not be repeated here. In addition to these caveats, our simulations of the 0–0 band of the O_2 atmospheric emission used the same chemistry as that of the 0–1 band, which produces a smaller VER than observed. However, because we are only interested in relative brightness fluctuations caused by linear waves, this assumption does not affect our results or conclusions.

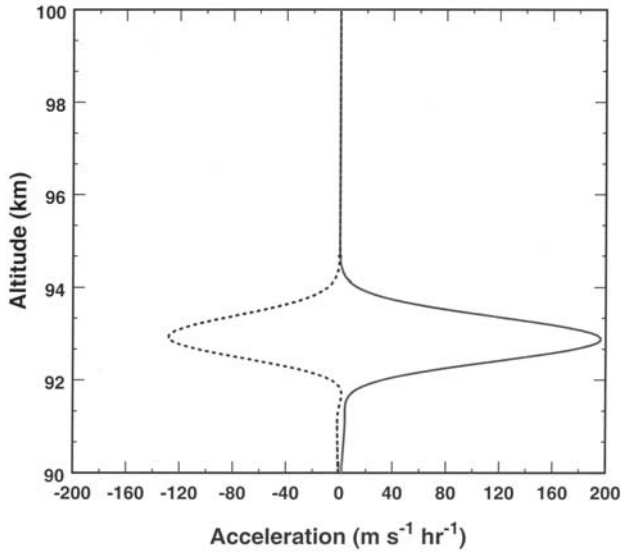

Figure 9. Mean state acceleration in the meridional (solid curve) and zonal (dashed curve) directions associated with the momentum flux divergence of wave C propagating in the nominal mean winds.

[32] Although all four of the waves considered in this study were observed by a ground-based imaging system during the ALOHA-93 campaign, our modeling has demonstrated that only one of these waves (wave C) could have been observed from space. The explanation for this is that wave C encountered a critical level within the airglow emission layer, limiting the VER fluctuations to a shorter distance along the satellite line of sight, and reducing the cancellation associated with different phases of the VER fluctuations along the line of sight. Wave A had a large vertical wavelength throughout the airglow emission regions, but significant cancellation occurred along the satellite line of sight for this wave because of the small horizontal wavelength (20 km) combined with significant VER fluctuations occurring over a long distance along the satellite line of sight. Therefore, the existence of a critical level lying within the airglow region appears to favor, and perhaps even facilitate, the observation of a wave from space in the airglow.

[33] The location of the critical region within the airglow region also leads to strong dissipation for such waves in the airglow region and to a strong forcing of the mean state at those levels. Our derived momentum flux per unit mass ($\sim$64 m^2 s^{-2} for wave C) is smaller than that derived from airglow and radar measurements by *Fritts et al.* [2002] ($\sim$900 m^2 s^{-2}), but is in general accord with values of $\sim$30 to 60 m^2 s^{-2} derived from radar measurements [e.g., *Fritts and Vincent*, 1987]. Our derived momentum flux convergence produced a mean state acceleration of $\sim$230 m s^{-1} hr^{-1} centered at $\sim$93 km altitude with a full-width at half-maximum of $\sim$1 km. If the forcing duration were limited to 10 min, this would equate to a maximum change in wind speed of $\sim$40 m s^{-1}, which is about half the value given by *Fritts et al.* [2002]. However, their wave was more energetic

than ours, and was assumed to produce a constant forcing over a broad region having a thickness of one scale-height, or ~6 km. In contrast to this, wave C forced the mean state over a very narrow region of the atmosphere due to its critical level interaction. In spite of this, the wave could have significantly modified the mean state because it was observed fairly continuously for several hours in the airglow during the ALOHA-93 campaign [M. J. Taylor, private communication, 2001]. The inferred long duration of forcing would necessitate time-dependent modeling to accurately describe the evolution of the mean state. However, our approach does provide an indication of the importance of waves observed in the airglow to the momentum budget of the MLT region.

[34] For wave C the momentum flux at 92 km altitude is $\sim 1.5 \times 10^{-4}$ J m^{-3}. In the absence of critical levels or dissipation, this value would remain approximately constant at lower altitudes and so can be tentatively compared with measurements made in the lower atmosphere. *Hertzog and Vial* [2001] have inferred an absolute value of momentum flux per unit mass of $\sim 10^{-2}$ m^2 s^{-2} at 20 km altitude in the equatorial lower stratosphere. This represents an average for gravity waves with periods between 1 hour and 1 day, and corresponds to a momentum flux of $\sim 8 \times 10^{-4}$ J m^{-3} at the same altitude. Therefore, our monochromatic high-frequency gravity wave (wave C) could have an associated momentum flux at low altitudes that is comparable to those associated with low-frequency motions. Differences between these two values of momentum flux can be attributed to the vastly different wave periods of the relevant motions, and may also be due a loss of momentum flux associated with wave C during propagating from the lower atmosphere (from its assumed source region) to the mesopause region. *Fritts and Vincent* [1987] noted from their observations that two thirds of the momentum flux was carried by waves with periods between 8 min and 1 hour (which would include wave C with a period of 9.5 min). *Alexander and Pfister* [1995] derived a low-latitude momentum flux of $\sim 1.2 \times 10^{-1}$ J m^{-3} at 18 km altitude, which represents an average for waves with horizontal wavelengths between 10 and 100 km (which again would include wave C with a horizontal wavelength of ~30 km). However, only a small fraction of this momentum flux would be expected to reach the mesopause region.

[35] Our derived energy flux for wave C is quite large ($\sim 10^{-2}$ W m^{-2}) below the critical region. This energy flux should be approximately conserved at lower altitudes, and so perhaps provides some information about the source strength for such waves in the troposphere. *Gossard* [1962] suggested that an energy flux of $\sim 10^{-1}$ W m^{-2} commonly leaves the troposphere. *Bertel et al.* [1978] and *Bertin et al.* [1978] observed dozens of gravity waves in the lower to middle thermosphere and concluded that the source for most of these waves was the meteorological jet stream. The inferred energy fluxes associated with these waves varied considerably around a mean value of $\sim 10^{-4}$ W m^{-2}. Calculations (not shown) suggest that the vertical energy flux associated with the wave discussed by *Fritts et al.* [2002] is ~0.2 W m^{-2}. Obviously there exists a wide range of possible energy fluxes associated with lower atmospheric sources, and our derived value for wave C ($\sim 10^{-2}$ W m^{-2}) is certainly not unreasonable.

[36] Knowledge of key wave parameters derived from ground-based airglow observations (horizontal wavelength, direction of propagation, wave extrinsic frequency, airglow perturbation amplitude, and also the altitude variation of the mean winds) has allowed us to model the waves observed in the airglow and, in the case of wave C, to deduce fluxes of energy and momentum as well as their divergence. To deduce quantities associated with the energetics of gravity waves using space-based observations will be a more challenging task. In principle the horizontal wavelength, direction of propagation, airglow perturbation amplitude, and altitude variation of the mean winds can all be measured from space-based experiments. Although it is not possible to measure wave frequency, it may be possible to infer the vertical wavelength from space-based observations by simultaneously acquiring airglow information from a set of various tangent ray heights. In that case the combination of modeling and space-based airglow observations could provide a means to infer wave amplitudes and phases as a function of height, from which information critical to deriving the mean state forcing could be extracted.

5. Conclusions

[37] We have used four sets of gravity wave parameters inferred from the ALOHA-93 campaign observations described previously by *Hickey et al.* [1998], and mean winds inferred from the lidar observations of *Gardner et al.* [1995] and *Tao and Gardner* [1995], to simulate the propagation of these gravity waves through the airglow layers in the mesopause region. By normalizing the wave amplitudes so that the modeled airglow response to the waves matched the measured response, we were able to derive the wave amplitudes as a function of altitude. We simulated space-based observations of these waves in the airglow emissions, and found that the only wave of the four that would be observable from space is the one that encountered a critical level within the lower region of the airglow layers. Therefore, the existence of a critical level lying within the lower region of an airglow layer appears to favor the observation of a wave from space.

[38] The 180° ambiguity in propagation direction associated with a space-based observation of a wave system appearing stationary to a fast-moving satellite, could be removed for the wave encountering a critical level in the airglow region. As noted by *Hickey and Brown* [2000] and *Brown and Hickey* [2001], it is serendipitous that waves whose direction can be determined from airglow observations are also those waves most likely to produce significant forcing of the mean state in the airglow region. For this particular wave we calculated the momentum flux, the energy flux, and the mean state acceleration associated with the critical level interaction, and found that the derived values agreed with generally accepted values. This demonstrates the usefulness of combining modeling with airglow observations of waves provided that simultaneously measured mean winds in the airglow region of interest are available.

[39] **Acknowledgments.** M. P. Hickey was supported by NASA grants NAG5-7592 and NAG5-10251 and NSF grant ATM-9816159. J. S. Brown was supported by NASA grant NAG5-7592.

[40] Arthur Richmond thanks Chester Gardner and another reviewer for their assistance in evaluating this manuscript.

References

Alexander, M. J., and L. Pfister, Gravity wave momentum flux in the lower stratosphere over convection, *Geophys. Res. Lett.*, *22*, 2029–2032, 1995.

Andrews, D. G., and M. E. McIntyre, Planetary waves in horizontal and vertical shear: The generalized Eliassen and Palm relation and the mean zonal acceleration, *J. Atmos. Sci.*, *33*, 2031–2048, 1976.

Bertel, L., F. Bertin, J. Testud, and D. Vidal-Madjar, Evaluation of the vertical flux of energy into the thermosphere from medium scale gravity waves generated by the jet stream, *J. Atmos. Terr. Phys.*, *40*, 691, 1978.

Bertin, F., J. Testud, L. Kersley, and P. R. Rees, The meteorological jet stream as a source of medium scale gravity waves in the thermosphere: An experimental study, *J. Atmos. Terr. Phys.*, *40*, 1161, 1978.

Breeding, R. J., A non-linear investigation of critical levels for internal atmospheric gravity waves, *J. Fluid Mech.*, *50*, 545, 1971.

Bretherton, F. P., and C. J. R. Garrett, Wave trains in inhomogeneous moving media, *Proc. R. Soc. London, Ser. A*, *302*, 529, 1968.

Brown, J. S., and M. P. Hickey, Gravity wave propagation directions inferred from satellite observations including smearing effects, *J. Geophys. Res.*, *106*, 3631–3643, 2001.

Eliassen, A., and E. Palm, On the transfer of energy in stationary mountain waves, *Geophys. Publ.*, *22*(3), 1–13, 1961.

Fritts, D. C., Gravity wave saturation in the middle atmosphere: A review of theory and observation, *Rev. Geophys.*, *22*, 275, 1984.

Fritts, D. C., and R. A. Vincent, Mesospheric momentum flux studies at Adelaide, Australia: Observations and a gravity wave-tidal interaction model, *J. Atmos. Sci.*, *44*, 605–619, 1987.

Fritts, D. C., S. L. Vadas, and Y. Yamada, An estimate of strong local body forcing and gravity wave radiation based on OH airglow and meteor radar observations, *Geophys. Res. Lett.*, *29*, doi:10.1029/2001GL013753, 2002.

Gardner, C. S., X. Tao, and G. C. Papen, Simultaneous lidar observations of vertical wind, temperature, density profiles in the upper mesosphere: Evidence for nonseparability of atmospheric perturbation spectra, *Geophys. Res. Lett.*, *22*, 2877–2880, 1995.

Gossard, E. E., Vertical flux of energy into the lower ionosphere from internal gravity waves generated in the troposphere, *J. Geophys. Res.*, *67*, 745, 1962.

Hecht, J. H., S. K. R. Howat, R. L. Walterscheid, and J. R. Isler, Observations of spectra of intensity fluctuations of the OH Meinel nightglow during ALOHA-93, *Geophys. Res. Lett.*, *22*, 2873–2876, 1995.

Hedin, A. E., Extension of the MSIS thermosphere model into the middle and lower atmosphere, *J. Geophys. Res.*, *96*, 1159, 1991.

Hertzog, A., and F. Vial, A study of the dynamics of the equatorial lower stratosphere by use of ultra-long duration balloons, 2, Gravity waves, *J. Geophys. Res.*, *106*, 22,745–22,761, 2001.

Hickey, M. P., and J. S. Brown, Resolving ambiguities in gravity wave propagation directions inherent in satellite observations: A simulation study, *Geophys. Res. Lett.*, *27*, 2901–2904, 2000.

Hickey, M. P., and R. L. Walterscheid, A note on gravity wave-driven volume emission rate weighted temperature perturbations inferred from O_2 atmospheric and OI 5577 airglow observations, *J. Geophys. Res.*, *104*, 4279–4286, 1999.

Hickey, M. P., R. L. Walterscheid, M. J. Taylor, W. Ward, G. Schubert, Q. Zhou, F. Garcia, M. C. Kelley, and G. G. Shepherd, Numerical simulations of gravity waves imaged over Arecibo during the 10-day January 1993 campaign, *J. Geophys. Res.*, *102*, 11,475, 1997.

Hickey, M. P., M. J. Taylor, C. S. Gardner, and C. R. Gibbons, Full-wave modeling of small-scale gravity waves using Airborne Lidar and Observations of the Hawaiian Airglow (ALOHA-93) O(^{1}S) images and coincident Na wind/temperature lidar measurements, *J. Geophys. Res.*, *103*, 6439–6453, 1998.

Hickey, M. P., R. L. Walterscheid, and G. Schubert, Gravity wave heating and cooling in Jupiter's thermosphere, *Icarus*, *148*, 266–281, 2000.

Larsen, M. F., Coqui 2: Mesospheric and lower thermospheric wind observations over Puerto Rico, *Geophys. Res. Lett.*, *27*, 445–448, 2000.

Larsen, M. F., Winds and shears in the mesosphere and lower thermosphere: Results from four decades of chemical release wind measurements, *J. Geophys. Res.*, *107*, doi:10.1029/2001JA000218, 2002.

Lindzen, R. S., *Dynamics in Atmospheric Physics*, Cambridge Univ. Press, New York, 1990.

Strobel, D. F., Constraints on gravity wave induced diffusion in the middle atmosphere, *Pure Appl. Geophys.*, *130*, 533, 1989.

Swenson, G. R., M. J. Taylor, P. J. Espy, C. Gardner, and X. Tao, ALOHA-93 measurements of intrinsic AGW characteristics using airborne airglow imager and ground-based Na wind/temperature lidar, *Geophys. Res. Lett.*, *22*, 2841–2844, 1995.

Tao, X., and C. S. Gardner, Heat flux observations in the mesopause region above Haleakala, *Geophys. Res. Lett.*, *22*, 2829–2832, 1995.

Taylor, M. J., E. H. Ryan, T. F. Tuan, and R. Edwards, Evidence of preferential directions for gravity wave propagation due to wind filtering in the middle atmosphere, *J. Geophys. Res.*, *98*, 6047, 1993.

Taylor, M. J., M. B. Bishop, and V. Taylor, All-sky measurements of short-period waves imaged in the OI(557.7 nm), Na(589.2 nm), and near-infrared OH and O_2(0,1) nightglow emissions during the ALOHA-93 campaign, *Geophys. Res. Lett.*, *22*, 2833–2836, 1995.

Zhu, X., P. K. Swaminathan, J. H. Yee, D. F. Strobel, and D. Anderson, A globally balanced two-dimensional middle atmosphere model: Dynamical studies of mesopause meridional circulation and stratosphere-mesosphere exchange, *J. Geophys. Res.*, *102*, 13,095–13,112, 1997.

J. S. Brown, Department of Physics and Astronomy, Clemson University, 600 S. Clyde Morris Boulevard, Clemson, SC 29634-0978, USA. (jsbrown@ces.clemson.edu)

M. P. Hickey, Department of Physical Sciences, Embry-Riddle Aeronautical University, Daytona Beach, FL 32114, USA.